Int. J. Heat Mass Transfer. Vol. 36, No. 3, pp. 783–791, 1993
Printed in Great Britain

0017-9310/93 $6.00 + 0.00

Augmentation of boiling heat transfer by utilizing the EHD effect—EHD behaviour of boiling bubbles and heat transfer characteristics

JUNJI OGATA
Mitsubishi Heavy Industries, Ltd, 2-1-1, Shinhama, Arai-cho, Takasago City, Japan

and

AKIRA YABE
Mechanical Engineering Laboratory, MITI 1-chome, Namiki, Tsukuba City, Japan

(*Received* 5 *April* 1991 *and in final form* 13 *December* 1991)

Abstract—In order to investigate the mechanism of augmentation of boiling heat transfer by utilizing electrohydrodynamic (EHD) phenomena, we performed basic experiments and analyses of bubble behaviour under applied electric fields and temperature gradients. These experiments clarified that the number of boiling bubbles increased greatly and they were forced to move around on the heat transfer surface violently, and that the area between the bubbles and heating surface effective for boiling heat transfer was enlarged.

1. INTRODUCTION

SINCE THE application of an electric field to thermal hydraulic phenomena was demonstrated to produce new phenomena called the electrohydrodynamic (EHD) effect, resulting in augmentation of heat transfer, a great deal of research has been conducted, primarily on augmentation of convective and condensation heat transfer. Some of this has been directed at practical applications. As for boiling heat transfer, however, due to the complexity of EHD effects during boiling, a qualitative understanding of this effect is lacking, and in many cases only experimental data have been reported [1–5]. In such reports the following phenomena have been described: the number of boiling bubbles may increase or decrease under an electric field; bubbles become charged, causing them to be attracted to electrodes. These phenomena seem to be related to the type and polarity of the electric fields. The fundamental mechanisms of these phenomena have not been reported.

In order to clarify the mechanisms of these phenomena and to establish a new method of augmenting boiling heat transfer, we have carried out basic experiments and analyses on the behaviour of bubbles under an electric field.

In a previous experiment on augmented boiling heat transfer in a smooth single tube boiling apparatus [6], a 25 kV source was used to apply an electric field to a mixture of ethanol and R-11, of which the relaxation time of the electric charges was smaller than the detachment period of the bubbles. Boiling heat transfer was augmented by about 8.5 times that without an electric field. To clarify the mechanism of augmentation, air bubble behaviour was observed under an electric field in adiabatic conditions. These experiments revealed that bubbles were deformed and pressed against the heat transfer surface, and were forced to move around violently on the surface by an electric field. This paper describes the results of experiments and analyses on the behaviour of bubbles in an electric field when temperature gradients exist.

2. EXPERIMENTS

Figure 1 shows the experimental apparatus used to observe bubble behaviour. This apparatus is nearly

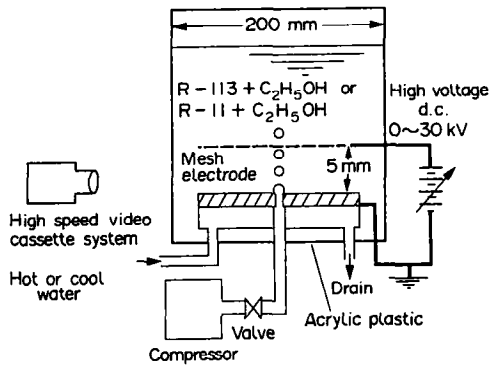

FIG. 1. Schematic diagram of experimental apparatus for observing bubble behaviour under electric fields.

NOMENCLATURE

ΔA	element of surface area [m^2]
d_e	equivalent diameter [m]
E	electric field strength [$V\ m^{-1}$]
j	electric current density [$A\ m^{-2}$]
k	Boltzmann constant [$eV\ K^{-1}$]
n	normal unit
P_D	electrostriction force [Pa]
P_E	electrostatic force [Pa]
P_M	Maxwell stress [Pa]
R	principal radius of curvature [m]
r	radial component of cylindrical coordinate
T	temperature [K]
W	activation energy [W]
z	vertical component of cylindrical coordinate.

Greek symbols

α	surface tension [$N\ m^{-1}$]
γ	fluid density [$kg\ m^{-3}$]
ε	relative dielectric constant
ε_0	absolute dielectric permittivity [$F\ m^{-1}$]
θ	angle [deg]
ξ	deformation length of bubble [m]
ρ_e	electric charge density [$C\ m^{-3}$]
σ_e	electrical conductivity [$A\ V^{-1}\ m^{-1}$]
ϕ	electrical potential [V].

Subscripts and superscripts

~	non-dimensional expression
0	base value
b	bubble
G	vapour
i	ith component
L	liquid
max	reference value (maximum value)
r	radial component
sat	saturation
z	vertical component.

the same as that described in the previous report [6]. A brass heat transfer surface 45 mm in diameter is installed in a cubic vessel made of acryl resin measuring 200 mm on each side. Water flows in the jacket below the heat transfer surface for heating and cooling. An electric heater is also used for heating instead of water. A brass screen of 25 mesh per inch is used for the upper electrode and its distance from the grounded heat transfer surface is 5 mm. Mixtures of R-113 and ethanol and R-11 and ethanol were used as the heat transfer media to make the relaxation time of the electric charge shorter. A mixture of R-113 and ethanol was used for the observation of air bubbles, while a mixture of R-11 and ethanol was used for the observation of air and boiling bubbles. A high speed VTR system (Kodak SP-2000) was used for these observations.

Figure 2 shows the experimental apparatus used to measure the boiling heat transfer of a mixture of R-11 and ethanol. This apparatus has a brass heat transfer surface 50 mm in diameter, surrounded by a teflon insulator 150 mm in outer diameter. It is located at the bottom of a vessel made of acrylic plate. The size of the vessel is 240 mm in width, 240 mm in length and 510 mm in height. A water-cooled condenser is located in the upper part of this vessel. The central part of the heat transfer surface consists of a brass bar 5 mm in diameter, with a 2 mm thick teflon insulator wrapped around it. In this brass bar, a total of five ϕ 0.5 mm K-type sheathed thermocouples are stacked horizontally 5 mm apart in the vertical direction to measure the heat flux. The thermal conductivity of the brass was measured by the laser flash method. In each

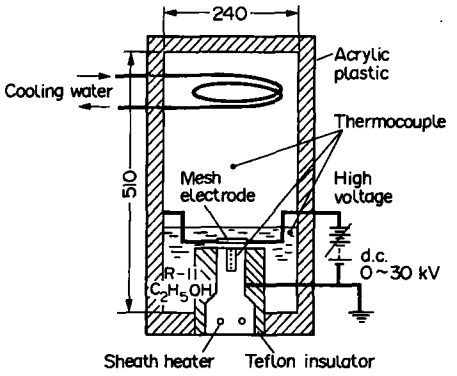

(a) Schematic diagram of experimental apparatus

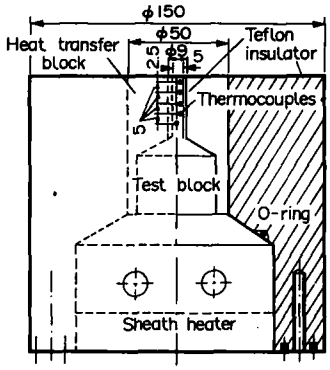

(b) Detail of heating section

FIG. 2. Experimental apparatus for measuring heat transfer characteristics under electric fields: (a) schematic diagram of experimental apparatus; (b) detail of heating section.

experiment, the brass heat transfer surface was polished with No. 2000 emery paper.

The experimental conditions in the vessel were as follows:

pressure	atmospheric
heat flux	3–50 kW m^{-2}
applied voltage	0–30 kV
(electric field strength)	0–6 MV m^{-1}
polarity of applied voltage	positive and negative d.c.

In addition, the alcohol concentration of the mixture was changed to observe the effect of electrical conductivity. To measure the electrical conductivity, a super insulating resistance meter was used.

3. EXPERIMENTAL RESULTS

In the experiment of heating air bubbles, a phenomenon different from that in the previous case of non-heating [6] was observed. Figure 3(a) shows photographs of the air bubble behaviour in the electric field. When there was no heating (i.e. under isothermal conditions), the bubbles were pressed against the lower electrode with a positive applied voltage and were not pressed with a negative applied voltage. On the other hand, when heated, the bubbles were pressed against the heat transfer surface serving as the lower electrode and moved violently around on it when either a positive or negative voltage was applied. In addition, more bubbles remained attached to the heat transfer surface in the heating condition than in the isothermal condition. When the heat transfer surface was cooled, no bubbles were attached to the heat transfer surface, irrespective of the polarity of the applied voltage.

In boiling of the R-11/ethanol mixture in the electric field, almost the same behaviour as was observed for air bubbles occurred, but it was entirely different from the phenomenon of nucleate boiling ordinarily observed without the electric field. When the applied voltage exceeds 10 kV, boiling bubbles are pressed

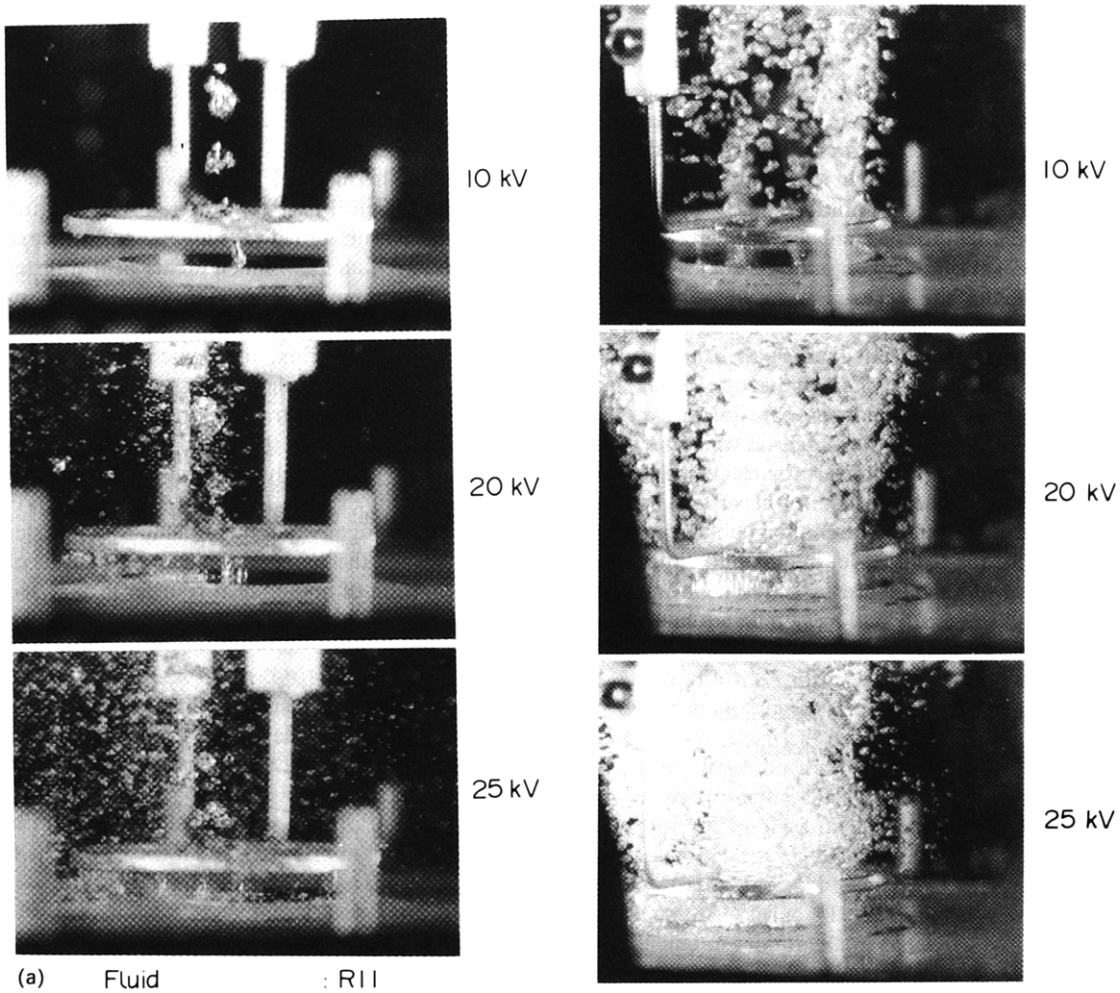

FIG. 3. (a) Air bubble behaviour in the electric field. (b) Boiling bubble behaviour of R-11 in the electric field.

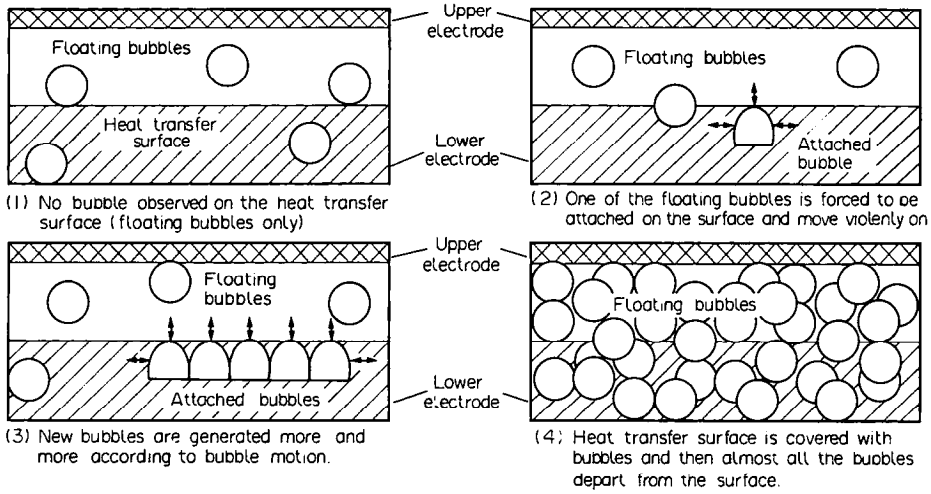

FIG. 4. Boiling bubble behaviour by observing high speed video recorder.

against the heat transfer surface and move violently around on it. When the applied voltage exceeds 20 kV, the diameter of the bubbles becomes smaller and they move more violently, simultaneously generating new bubbles by break-up on the heat transfer surface. The generated bubbles also move violently around the heat transfer surface, producing new bubbles. A sketch of such bubble behaviour is shown in Fig. 4. Initially there are no bubbles on the heat transfer surface and only the floating bubbles exist in the electric field. Then one of the floating bubbles becomes attached to the heat transfer surface by the electric force, and the bubble begins to move violently on the surface. Soon after, it splits into smaller bubbles that continue moving violently and they soon grow as large as the mother bubble and also split into new small bubbles. Consequently, when the heat transfer surface becomes covered with bubbles, the electric field cannot keep the bubbles attached to the surface because the electric field strength around the bubbles becomes weaker, allowing them to float in the bulk liquid.

The shape of the bubble attached to the heat transfer surface is semi-ellipsoidal with a spread bottom. Its gas–liquid interface is severely perturbed. The bubble diameter decreases as the applied voltage increases and the rise-up velocity of the bubble increases. The boiling heat transfer characteristics are shown in Fig. 5. This figure also displays data for pure R-11 on other high-performance heat transfer surfaces, such as the commercial 'Thermoexcel' [7] machined porous surface, the 'High Flux' [8] sintered surface and another sintered surface with the highest performance [9]. The present data show much higher heat transfer rates than these high-performance surfaces, demonstrating the high EHD effect on boiling enhancement.

For the same heat flux, the degree of superheat decreases when the applied voltage increases. In addition, the boiling heat transfer rate depends on the electrical conductivity of the liquid, as indicated in Fig. 6, and becomes nearly constant when the electrical conductivity exceeds 7×10^{-8} (A V^{-1} m^{-1}). As shown in Fig. 6, augmentation of boiling heat transfer reaches 50 times the base value. The mechanism of the augmentation of boiling heat transfer is analysed

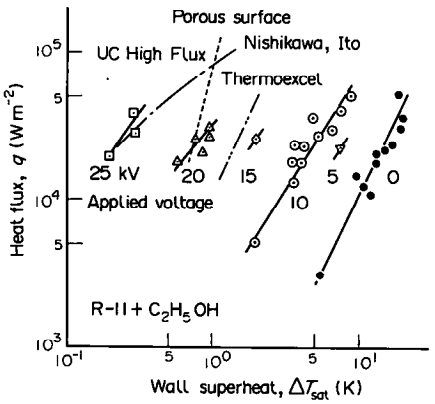

FIG. 5. Experimental results of boiling characteristics (boiling curves).

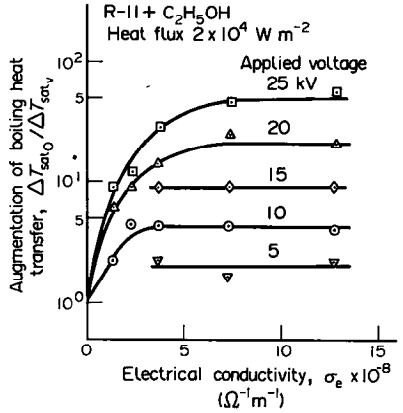

FIG. 6. Relationship between augmentation of boiling heat transfer and electrical conductivity of fluid.

using the conceptual model described in the next section.

4. ANALYSIS

4.1. *Models for augmented boiling heat transfer*

From the observation of air bubble and boiling bubble behaviour in an electric field, the following model for augmented boiling heat transfer is proposed:

(1) Inside the thermal boundary layer, the bubbles are pushed toward the heat transfer surface under the applied voltage and pressed against it by the electrostatic force. The bottom of the bubble spreads out on the heat transfer surface causing an increase in the area of the thin liquid film beneath the bottom of the bubble.

(2) Bubbles move violently around on the heat transfer surface and generate new bubbles by break-up of old bubbles, thereby increasing the number of bubbles on the heat transfer surface. To put it concretely, increase of the applied voltage causes the bubble diameter to decrease and, at a constant heat flux, the number of bubbles moving around the heat transfer surface increases and a maximum increase in the number of bubbles present on the surface occurs under the maximum applied voltage.

These models are discussed in the following sections.

The reason why the bubbles are pressed against the heat transfer surface is discussed in the following. Figure 7 shows the force in the electric field that acts on the bubbles in the thermal boundary layer. Because the electrical conductivity, σ_e, is temperature dependent, electric charges are created in the thermal boundary layer. Representating the gradient of electrical conductivity by $\nabla\sigma_e(T)$, the charge density can be expressed as

$$\rho_e = -\frac{\varepsilon_0\varepsilon}{\sigma_e} E\cdot\nabla\sigma_e(T). \quad (1)$$

Therefore, when the upper electrode is positive a negative charge is generated in the superheated layer, and when the polarity is negative a positive charge is generated. In addition, the electric field strength of the superheated layer becomes weaker than that of the saturated liquid. In contrast, due to the difference in the dielectric constants between the gas phase and the liquid phase, a dielectrophoretic force acts on the dielectrics. Since $\varepsilon_L > \varepsilon_G$, bubbles tend to move away from the stronger electric field toward the weaker electric field if the electric current is assumed to be constant. Consequently the bubbles are pressed against the heat transfer surface. In the case of cooling, the electric field strength in the thermal boundary layer is larger, so that the bubbles are not pressed against the heat transfer surface. The latter effect was confirmed experimentally under a cooling condition.

In addition, because the electric field strength in the superheated layer is weaker than in the saturated fluid, the electrostatic force acting on the liquid–bubble interface weakens. Assuming that the bubbles are isobaric and their volumes remain constant, the bubbles are compressed at the saturated fluid interface by the electrostatic force, becoming more slender in the middle and broader at the bottom. The result is that the bubbles are elongated in the superheated layer.

The reason why an increase in electrical conductivity causes an increase in the augmented heat transfer rate is discussed as follows. As the electrical conductivity increases, the boiling heat transfer is greatly augmented because the relaxation time of the electric charge becomes sufficiently smaller than the detachment period of bubbles. However, the bubble detachment period itself becomes shorter because the applied voltage is increased. Therefore, the value of the electrical conductivity increases to maintain the highest value of the augmentation of heat transfer rate.

The reason why the bubble diameter decreases and the number of bubbles on the heat transfer surface increases as the applied voltage increases is as follows. The bubbles pressed against the heat transfer surface move violently around on the heat transfer surface by an electrostatic force, causing faster growth of bubbles by evaporation of the thin liquid films between the bottoms of the bubbles and the heat transfer surface. However, due to the EHD instability at the liquid–bubble interface, a bubble cannot grow beyond a critical diameter (derived from the Taylor instability criterion), and the bubble splits into smaller bubbles, causing an increase in the number of bubbles on the heat transfer surface. Also, the bottom of each bubble spreads due to the electrostatic force, thereby increasing the heat transfer area. This is considered to be another reason for the large enhancement of heat transfer.

Observation with a high speed VTR indicated a reduction in the number of bubbles on the heat transfer surface several times per second. This occurs when the bubbles fill the gap between the upper electrode and the grounded heat transfer surface, varying the distribution of electrical potential. This weakens the electrostatic force on the bubbles, allowing them to be released from the surface due to buoyancy. As the number of bubbles on the heat transfer surface decreases, the electrostatic force acting on the bubbles increases, so that the bubbles are again pressed against the heat transfer surface. These bubbles move around violently and new bubbles are generated by fracture.

With regard to the mechanism of augmented heat transfer utilizing EHD effects in the nucleate boiling region, the parameters related to properties of the heat transfer surface such as surface roughness and nucleation site density are not important. In contrast, the EHD effect on the behaviour of bubbles on the

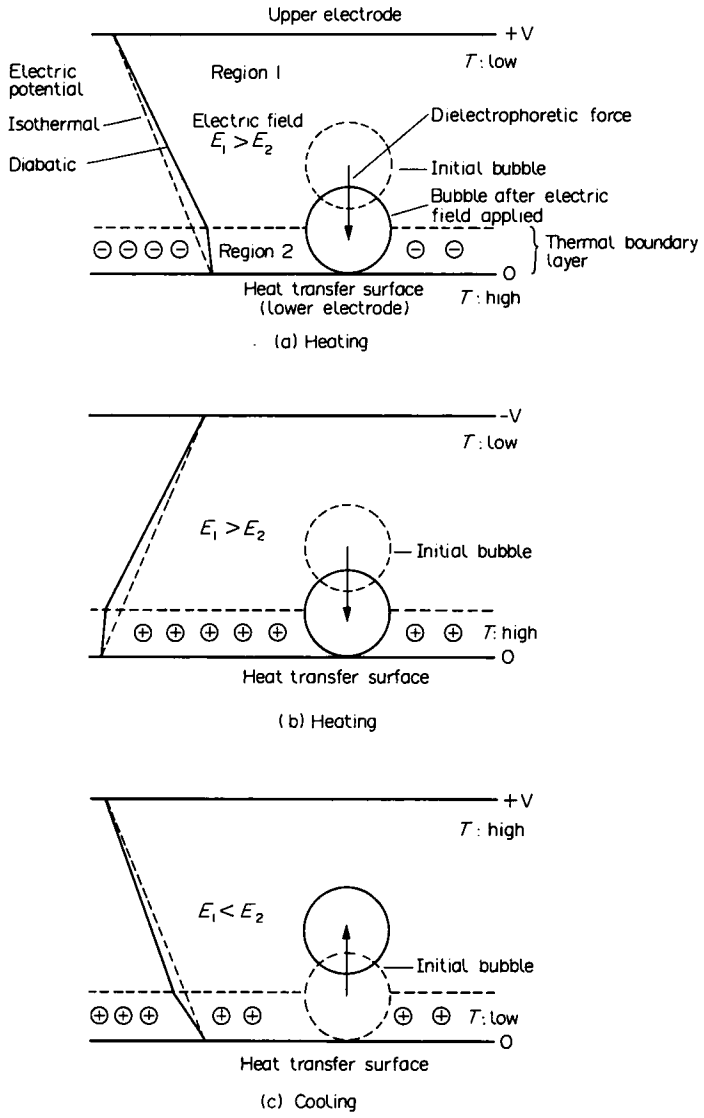

FIG. 7. Model of bubble behaviour affected by the electrostatic force.

heat transfer surface is important. In other words, the initial bubbles may be generated by a variety of mechanisms: at active cavities on the heat transfer surface; formed by bubbles at both ends of the heat transfer surface; in the groove of the spacer between the electrodes where the local heat flux is higher; and floating bubbles in the liquid. In whatever way they are formed, the EHD effect makes these bubbles be pressed against the heat transfer surface, resulting in the effects mentioned above. Furthermore, a bubble break-up that occurs on the heat transfer surface leads to the generation of smaller bubbles, and each bubble repeats this growth and break-up process independently of the properties of the heat transfer surface. This should be an excellent feature for practical applications.

In the preceding report [6], the mechanism wherein the bubbles move violently on the heat transfer surface was described by an analysis of the electric field affecting the bubbles. A fundamental analysis of the shape of the bubbles on the heat transfer surface is described in the following.

4.2. *Analysis of electrical potential distribution around a bubble*

Considering the relationship between the charge relaxation time and the detachment period of generated bubbles, the liquid can be treated as an electrical conductor. Because the flow velocity is small, we neglect the term for the convective electric current so that the basic equations can be expressed as follows:

(i) continuity equation of electric current

$$\nabla \cdot j = 0 \tag{2}$$

(ii) Ohm's law

$$j = \sigma_e E \tag{3}$$

(iii) definition of electrical potential

$$E = -\nabla\phi. \tag{4}$$

By adopting the cylindrical coordinates, we define the following dimensionless variables:

applied voltage $\tilde{\phi} = \phi/\phi_{max}$
distance between electrode $\tilde{z} = z/z_{max}$
radial distance $\tilde{r} = r/r_{max}$.

With these dimensionless variables the boundary conditions are

(i) $$\tilde{\phi} = 0 \quad \text{at} \quad \tilde{z} = 0. \tag{5}$$

(ii) $$\tilde{\phi} = 1 \quad \text{at} \quad \tilde{z} = 1. \tag{6}$$

(iii) When $\tilde{z} \geqslant z_b$, at $\tilde{r} = 0$ and $\tilde{r} = 1$

$$\frac{\partial\tilde{\phi}}{\partial\tilde{r}} = 0 \tag{7}$$

(iv) In the direction normal to the liquid–bubble interface

$$\frac{\partial\tilde{\phi}}{\partial n} = 0. \tag{8}$$

Furthermore, at the edge of the thermal boundary layer,

(v) $$D_{1n} = D_{2n} \tag{9}$$

and

(vi) $$E_{1t} = E_{2t}. \tag{10}$$

Since the dielectric constant of the liquid can be regarded as almost constant compared to the electrical conductivity for a given temperature change, the basic equations inside the thermal boundary layer differ from those outside it. By substituting equation (3) into equation (2) we obtain an expression that is valid inside the thermal boundary layer:

$$\nabla\cdot(\sigma_e E) = 0. \tag{11}$$

Substituting equation (4) into equation (11) yields

$$\nabla^2\phi + \frac{\nabla\sigma_e}{\sigma_e}\cdot\nabla\phi = 0. \tag{12}$$

Outside of the thermal boundary layer, $\nabla\sigma_e = 0$, so equation (12) reduces to

$$\nabla^2\phi = 0. \tag{13}$$

The electrical conductivity can be expressed as a function of temperature as

$$\sigma_e = \sigma_{e0}\, e^{-(W/kT)} \tag{14}$$

where W is the activation energy [10].

Therefore, when a Taylor expansion is made for small variations of temperature T_0, and substituting $\kappa = W/kT_0^2$, equation (14) can be approximated as $\sigma_e = \sigma_{e0}\{1+\kappa(T-T_0)\}$. The gradient of σ_e can therefore be expressed as

$$\nabla\sigma_e = \frac{\partial\sigma_e}{\partial T}\frac{\partial T}{\partial z} = \sigma_{e0}\kappa\frac{\partial T}{\partial z}. \tag{15}$$

Therefore, equation (15) can be expressed as

$$\frac{\nabla\sigma_e}{\sigma_e} = \frac{\kappa}{1+\kappa(T-T_0)}\frac{\partial T}{\partial z}. \tag{16}$$

The temperature distribution inside the thermal boundary layer is approximated by the following cubic polynomial of z:

$$\frac{T(z)-T_{sat}}{\Delta T_{sat}} = \left(1-\frac{z}{\delta}\right)^2\left(1+\frac{z}{\delta}\right) \tag{17}$$

where $\Delta T_{sat} = T_w - T_{sat}$. Taking the derivative of equation (17) with respect to z, we obtain

$$\frac{\partial T}{\partial z} = -\frac{\Delta T}{\delta}\left(1-\frac{z}{\delta}\right)\left(1+\frac{3z}{\delta}\right). \tag{18}$$

Using equations (16) and (18), equation (12) can be expressed as

$$\nabla^2\phi + a\cdot\nabla\phi = 0 \tag{19}$$

where

$$a = \frac{\Delta T}{\delta}\left(1-\frac{z}{\delta}\right)\left(1+\frac{3z}{\delta}\right)\frac{\kappa}{1+\kappa(T-T_0)}. \tag{20}$$

Expressing equation (19) in cylindrical coordinates yields

$$\frac{1}{r}\frac{\partial}{\partial r}\left(r\frac{\partial\phi}{\partial r}\right) + a\frac{\partial\phi}{\partial z} + \frac{\partial^2\phi}{\partial z^2} = 0. \tag{21}$$

Similarly, for conditions outside the thermal boundary layer, equation (13) can be expressed in cylindrical coordinates as

$$\frac{1}{r}\frac{\partial}{\partial r}\left(r\frac{\partial\phi}{\partial r}\right) + \frac{\partial^2\phi}{\partial z^2} = 0. \tag{22}$$

Consequently, by solving equations (21) and (22) the distribution of the electric potential is obtained.

From equations (9) and (10), the boundary conditions of the electric displacement vector and electric field strength at the edge of the thermal boundary layer are obtained as

$$\varepsilon_1\frac{\partial\phi_1}{\partial n} = \varepsilon_2\frac{\partial\phi_2}{\partial n} \tag{23}$$

and

$$\frac{\partial\phi_1}{\partial r} = \frac{\partial\phi_2}{\partial r} \tag{24}$$

respectively.

4.3. *Analysis of the bubble shape*

From the distribution of the electric potential obtained with equations (21)–(24), the bubble shape

is obtained considering the pressure balance between the electrostatic forces (Maxwell stress and electrostriction force) and the surface tension.

That is, the bubble radius, R, is obtained as

$$\frac{2\alpha}{R}+\left\{\frac{\varepsilon_0}{2}(\varepsilon_L-\varepsilon_G)E^2+\frac{\varepsilon_0}{2}\gamma_L\frac{\partial\varepsilon_L}{\partial\gamma_L}E^2\right\}=\text{constant}. \tag{25}$$

By rewriting the electrostriction force of the third term of the left-hand side of equation (25) using the Clausius–Mossotti relationship of

$$\frac{\varepsilon_L-1}{\varepsilon_L+2}=C\cdot\gamma_L. \tag{26}$$

Assuming that the first term on the left-hand member is $R=R_0+\xi$ (R_0, radius of initial shape), and by rewriting equation (25) using spherical coordinates assuming that a bubble is spherically symmetric, we obtain

$$\frac{2\alpha}{R_0}\left\{2\xi+\frac{1}{\sin\theta}\frac{\partial}{\partial\theta}\left(\sin\theta\frac{\partial\xi}{\partial\theta}\right)\right\}+\frac{\varepsilon_0}{2}(\varepsilon_L-\varepsilon_G)E^2$$

$$+\frac{\varepsilon_0}{6}(\varepsilon_L-1)(\varepsilon_L+2)E^2=\text{constant}. \tag{27}$$

The constant on the right-hand side of equation (27) is equivalent to the pressure increase caused by the electrostatic force. Equation (27) is solved by considering the pressure to be constant. It is based on the assumption that the volume of the bubble would be constant, since the pressure increase caused by the electrostatic force would be negligibly small compared with the atmospheric pressure. Figures 8(a) and (b) show the shape of bubbles obtained by considering the effect of the electrostatic force on the gas–liquid interface and by solving equation (27). The numerical calculations were conducted under the conditions that $\kappa=0.05$ ($^\circ C^{-1}$), which corresponds to a mixture of R-11 and ethanol with a 24:1 weight ratio, one-third of the bubble height as the thickness of the thermal boundary layer, 30% of the distance between electrodes as the height of the bubble and 0.5°C as the degree of superheat of the heat transfer surface. While no changes in the shapes of the bubbles were observed at an applied voltage of 10 kV, the bottom of the bubble spreads in the thermal boundary layer at 25 kV. These simulations indicate that the heat transfer area of the thin liquid film at the bottom of a bubble is enlarged and the change in the shape of bubble observed in the experiment is confirmed.

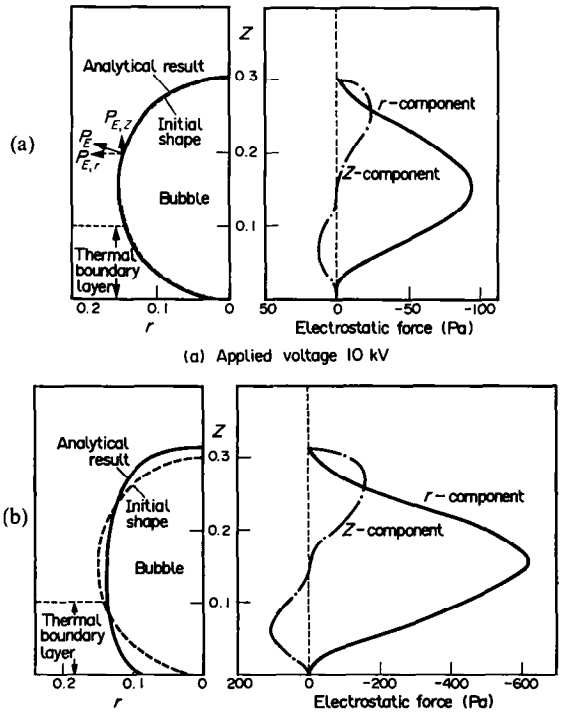

FIG. 8. Analytical results of bubble deformation and electrostatic force on the bubble: (a) applied voltage 10 kV; (b) applied voltage 25 kV.

5. CONCLUSIONS

The purpose of this study was to investigate the effect of an applied electric field on augmentation of heat transfer by nucleate boiling and to clarify the mechanism responsible for the effect. An experiment on pool boiling heat transfer on an upward-facing horizontal surface and an analysis of bubbles in an electric field when a thermal boundary layer exists were carried out.

From the experiment and analysis, the following points were clarified:

(1) When the heat transfer surface is heated, the bubbles in the electric field are pressed against the surface independently of the polarity of the electric field and move violently on and around the heat transfer surface. On the other hand, the bubbles are not pressed against the surface when it is cooled.

(2) It was shown that the boiling bubbles broke up and generated many new bubbles by moving violently around on the heat transfer surface, thereby leading to a drastic increase in the number of bubbles. This was the main cause for augmentation of heat transfer.

(3) It was demonstrated that the heat transfer performance was augmented as the electrical conductivity increased and became almost constant at electrical conductivities higher than 7×10^{-7} ($A\,V^{-1}\,m^{-1}$). The heat transfer augmentation reached a maximum of 50 times.

(4) The bubble deformed in the electric field to have a spread bottom on the heat transfer surface. An analytical simulation indicated that this shape was formed because a superheated liquid layer caused a weaker electric field strength than in the saturated region, resulting in a weaker electric force, and because of the internal pressure balance of a bubble. Also, it was predicted that the area of thin liquid film at the bottom of a bubble was enlarged by this bubble shape, giving rise to augmented heat transfer.

Acknowledgement—We wish to express our appreciation to

Professor Hideki Nariai of Tsukuba University, who offered us valuable advice during the course of this research.

REFERENCES

1. E. Bonjour *et al.*, Electroconvection effects on heat transfer, *Chem. Engng Prog.* **58,** 63–66 (1962).
2. P. H. G. Allen *et al.*, The potential of electrically enhanced evaporators, *3rd Int. Symp. on the Large Scale Applications of Heat Pumps*, pp. 221–229 (1987).
3. V. Asch, Electrokinetic phenomena in boiling Freon-113, *J. Appl. Phys.* **37,** 2654–2658 (1966).
4. T. Yokoyama *et al.*, Effect of an electric field on boiling heat transfer of fluorocarbon R-11, *XVIII Int. Centre for Heat and Mass Transfer* (Edited by J. Bouguard), p. 140. Hemisphere, New York (1987).
5. H. Kawahira *et al.*, Effect of an electric field in boiling heat transfer of refrigerant-11—boiling on a single tube, *IEEE Trans. Ind. Applic.* **26,** 359 (1990).
6. J. Ogata and A. Yabe, Basic study on the enhancement of nucleate boiling heat transfer by applying electric fields, *Int. J. Heat Mass Transfer* **36,** 775–782 (1993).
7. H. Kuwahara *et al.*, *14th Heat Transfer Symp. of Japan*, p. 121 (1977) (in Japanese).
8. P. S. O'Neil *et al.*, *Adv. Cryogen. Engng* **17,** 420 (1976).
9. K. Nishikawa *et al.*, Heat transfer in energy problems, *Proc. Japan and U.S. Joint Seminar*, p. 119 (1980).
10. I. Adamczewsky, *Ionization, Conducting and Breakdown in Dielectric Liquids*, p. 179. Taylor and Francis (1969).